

## DUST IN THE EXTREMELY METAL-POOR BLUE COMPACT DWARF GALAXY I Zw 18: THE SPITZER MID-INFRARED VIEW

YANLING WU<sup>1</sup>, V. CHARMANDARIS<sup>2,3</sup>, L. K. HUNT<sup>4</sup>, J. BERNARD-SALAS<sup>1</sup>, B. R. BRANDL<sup>5</sup>, J. A. MARSHALL<sup>1</sup>, VIANNEY LEBOUTEILLER<sup>1</sup>, LEI HAO<sup>1</sup>, J. R. HOUCK<sup>1</sup>*Accepted by ApJ, March 9th, 2007*

## ABSTRACT

I Zw 18, a blue compact dwarf (BCD) galaxy with the 2nd lowest metallicity measured in a star-forming object, has been observed with all three instruments on board the Spitzer Space Telescope. We present the deepest 5–36  $\mu\text{m}$  mid-infrared (mid-IR) spectrum of this galaxy as yet obtained, as well as 3.6  $\mu\text{m}$  to 70  $\mu\text{m}$  imaging results. As with SBS 0335-052E, another BCD with similar metallicity, I Zw 18 shows no detectable emission from polycyclic aromatic hydrocarbons (PAHs). However, the continuum emission, from 15 to 70  $\mu\text{m}$ , of I Zw 18 has a much steeper slope, more characteristic of a typical starburst galaxy of solar abundance. The neon abundance as measured from the infrared fine-structure lines is  $\sim 1/23 Z_{\odot}$ , and the sulfur abundance is  $\sim 1/35 Z_{\odot}$ , generally consistent with the nebular oxygen abundance of  $1/30 Z_{\odot}$  derived from optical lines. This suggests that the extinction to the infrared emitting regions of this galaxy is low, also in agreement with the optical Balmer line ratios.

*Subject headings:* dust, extinction — galaxies: individual (I Zw 18) — galaxies: dwarf — galaxies: starburst

## 1. INTRODUCTION

Low-metallicity galaxies may have been the first sites of star formation in the early universe (White & Rees 1978; Dekel & Silk 1986). Consequently understanding their properties may provide valuable insights into the formation of the first generation of normal stars and the subsequent enrichment of the interstellar medium. However, finding truly primordial galaxies in the distant universe is beyond the reach of current technology. At high redshift, observational limitations introduce biases toward the detection of high-mass high-luminosity systems in which the short time-scales of massive star formation lead to the identification of systems that are already chemically enriched (i.e., Maiolino et al. 2003). An alternative approach is to identify and study unevolved galaxies in the local universe. Such a sample are the blue compact dwarf galaxies (see the review by Kunth & Östlin 2000).

Since its discovery by Zwicky (1966) and the seminal paper of Searle & Sargent (1972), I Zw 18 has been studied extensively at many wavelengths. With an oxygen abundance determined from the optical lines in HII regions of  $12+\log(\text{O/H})=7.17$  (Skillman & Kennicutt 1993; Izotov & Thuan 1999), or  $\sim 1/30 Z_{\odot}$ <sup>6</sup>, it has remained the lowest metallicity BCD

for over two decades until the recent study of the western component of SBS 0335-052 (Izotov et al. 2005; Papaderos et al. 2006), which has slightly lower metallicity ( $12+\log(\text{O/H})=7.12$ ). Distance estimates to I Zw 18 range from  $\sim 10$  Mpc (Hunter & Thronson 1995),  $\sim 12.6$  Mpc (Östlin 2000), and up to  $\sim 15$  Mpc (Izotov & Thuan 2004). Here we adopt a distance of 12.6 Mpc ( $1'' \sim 61$  pc). I Zw 18 consists of two bright knots of star-formation, a northwest (NW) component and a southeast (SE) one, together they form the “main body” of the system. Both the NW and SE components contain numerous young star clusters, with ages ranging from 3 to 10 Myr, but the age of the underlying stellar population in I Zw 18 is still a matter of debate, with maximum ages ranging from 500 Myr to 5 Gyr (Aloisi et al. 1999; Östlin 2000; Recchi et al. 2002; Hunt et al. 2003; Izotov & Thuan 2004; Momany et al. 2005). Approximately 22'' northwest of the “main body”, there is a blue irregular low surface brightness star-forming region, called the “C component”, which is embedded in a common HI envelope (van Zee et al. 1998; Izotov & Thuan 2004).

It is well known that some BCDs are forming stars at a rate that can only be maintained for  $\sim 1/10$  of Hubble time given their store of available hydrogen. SBS 0335-052E, which has a similar metallicity ( $12+\log[\text{O/H}]=7.31$ ), is forming stars at a high rate in dense compact regions (Houck et al. 2004b). I Zw 18 is forming stars at a slower rate in complexes which are diffuse and extended (Hunt et al. 2005a). These differences have been attributed to different star-formation modes. SBS 0335-052E is in an “active” mode with relatively high star-formation rate (SFR) in compact dense regions, while in I Zw 18 star-formation occurs in a “passive” mode in more extended regions with a relatively low SFR (Hirashita & Hunt 2004).

In this paper, we present a detailed analysis of the in-

Electronic address: wyl@astro.cornell.edu, vassilis@physics.uoc.gr, hunt@astrotri.cornell.edu, jam258@cornell.edu

<sup>1</sup> Astronomy Department, Cornell University, Ithaca, NY 14853<sup>2</sup> University of Crete, Department of Physics, GR-71003, Heraklion, Greece<sup>3</sup> IESL/Foundation for Research and Technology - Hellas, GR-71110, Heraklion, Greece, and Chercheur Associé, Observatoire de Paris, F-75014, Paris, France<sup>4</sup> INAF-Istituto di Radioastronomia, Largo E. Fermi 5, 50125 Florence, Italy<sup>5</sup> Leiden Observatory, Leiden University, P.O. Box 9513, 2300 RA Leiden, The Netherlands<sup>6</sup> Izotov & Thuan (1999) give  $1/50 Z_{\odot}$ . Here, we use the new oxygen solar abundance of  $12+\log[\text{O/H}]=8.69$  (Allende Prieto et al. 2001), which results in a metallicity of  $1/30 Z_{\odot}$ .

frared properties of the “main body” of I Zw 18 based on the current deepest mid-IR spectra for this galaxy, obtained using the infrared spectrograph (IRS, Houck et al. 2004a) on the Spitzer Space Telescope (Werner et al. 2004). We also discuss the results of photometric observations with IRAC (Fazio et al. 2004) and MIPS (Rieke et al. 2004) observations. We describe the observation and data analysis in §2. The Spitzer images and spectra are discussed in §3, along with the observed morphologies and abundance estimates. A discussion of the SFR of I Zw 18 is given in §4 and we summarize our conclusions in §5.

## 2. OBSERVATIONS

### 2.1. *Spitzer/IRS Spectroscopy*

I Zw 18 was observed as part of the IRS<sup>7</sup> Guaranteed Time Observation program on 27 March 2004 using all four instrument modules. It was re-observed on 23 April 2005 with the short-low (SL) and long-low (LL) modules with increased integration time to achieve a higher signal-to-noise ratio (SNR) over the  $5 - 36 \mu\text{m}$  mid-IR continuum. A third even longer observation was made on 16 December 2005 with all four IRS modules. The target was acquired using the  $22\mu\text{m}$  (red) peak-up camera in high-accuracy mode, and the details of the observations are presented in Table 1.

The data were processed at the *Spitzer* Science Center (SSC) (pipeline version 14.0). The two-dimensional image data were converted to slope images after linearization correction, subtraction of darks, and cosmic-ray removal. Finally, the data were co-added. In order to increase the SNR of the subtracted background for SL and LL, we combined the background observed in off-order and off-nod positions. A detailed explanation for this method on faint source extraction can be found in Weedman et al. (2006). After subtracting the background, the one-dimensional spectra were extracted from images with a script version of the Spectral Modeling, Analysis and Reduction Tool (SMART, ver. 6.0.4, Higdon et al. (2004)). We used tapered column extraction starting from intermediate pipeline product droop files, which only lack stray light and flat-field correction. The data from short-high (SH) and long-high (LH) droop files used the full slit extraction method from the mean of the combined images. We calibrated the flux densities by multiplying the extracted spectrum with the relative spectral response function (RSRF), which was created from the IRS standard stars, HR6348 for SL, HD173511 for LL and  $\xi$  Dra for SH and LH, for which accurate templates are available (Cohen et al. 2003).

### 2.2. *Spitzer Imaging with IRAC and MIPS*

The galaxy was imaged at  $3.6, 4.5, 5.8$  and  $8\mu\text{m}$  using IRAC on 3 April 2004, as well as at  $24, 70$  and  $160\mu\text{m}$  using MIPS on 7 April 2004 (Engelbracht et al. 2005) (PID:59) (See Table 1). The IRAC high dynamic range mode was used with a 4 point small cycling pattern of 30 seconds exposure time for each frame. This resulted in an on-source time of 120 seconds for each IRAC filter. The MIPS photometry mode was used in small fields with 1

<sup>7</sup> The IRS was a collaborative venture between Cornell University and Ball Aerospace Corporation funded by NASA through the Jet Propulsion Laboratory and the Ames Research Center.

TABLE 1  
SPIZER OBSERVATIONS OF I Zw 18

| AORKEY   | Date       | Instrument                | On-source Time (sec) |
|----------|------------|---------------------------|----------------------|
| 9008640  | 2004-03-27 | IRS (SL)                  | 84                   |
|          |            | IRS (LL)                  | 120                  |
|          |            | IRS (SH)                  | 240                  |
|          |            | IRS (LH)                  | 120                  |
| 4330759  | 2004-04-03 | IRAC ( $3.6\mu\text{m}$ ) | 120                  |
|          |            | IRAC ( $4.5\mu\text{m}$ ) | 120                  |
|          |            | IRAC ( $5.8\mu\text{m}$ ) | 120                  |
|          |            | IRAC ( $8.0\mu\text{m}$ ) | 120                  |
| 4349184  | 2004-04-07 | MIPS ( $24\mu\text{m}$ )  | 48                   |
|          |            | MIPS ( $70\mu\text{m}$ )  | 231                  |
|          |            | MIPS ( $160\mu\text{m}$ ) | 42                   |
| 12622848 | 2005-04-23 | IRS (SL)                  | 480                  |
|          |            | IRS (LL)                  | 240                  |
| 16205568 | 2005-12-16 | IRS (SL)                  | 2040                 |
|          |            | IRS (LL)                  | 840                  |
|          |            | IRS (SH)                  | 2880                 |
|          |            | IRS (LH)                  | 1440                 |

cycle  $\times$  3 seconds at  $24\mu\text{m}$  and 2 cycles  $\times$  10 seconds at both  $70$  and  $160\mu\text{m}$ . Two offset positions ( $\pm 12''$ ) were used to allow proper subtraction of bad pixels. The total on-source times were 48, 231 and 42 seconds for the MIPS  $24, 70$  and  $160\mu\text{m}$  bands. The imaging data were processed by the SSC pipeline version 14.0 and the final mosaics were obtained from the Spitzer archive.

## 3. RESULTS

### 3.1. *Mid-IR Morphology*

Many ground-based and space-born instruments have been used to obtain optical/UV to near-IR data for I Zw 18 (Hunter & Thronson 1995; Aloisi et al. 1999; Östlin 2000; Cannon et al. 2002; Hunt et al. 2003; Izotov & Thuau 2004). Hunter & Thronson (1995) first resolved the “main body” of I Zw 18 into stars using the *Hubble* Space Telescope (HST). They have also detected filaments of ionized gas up to 450 pc from the center of the galaxy. Keck II spectra revealed H $\alpha$  emission as far as  $\sim 1800$  pc from the “main body” of I Zw 18. Izotov et al. (2001) have also shown that the equivalent widths of emission lines are large in this extended envelope. This, together with the optical and near-IR colors, suggests that ionized gas dominates the emission in the outermost regions.

In Figure 1 we present images of the “mainbody” of I Zw 18 in four infrared bands ( $3.6, 4.5, 8$  and  $24\mu\text{m}$ ). At  $3.6\mu\text{m}$ , where most of the light is due to the stellar photospheric emission, the morphology of I Zw 18 is very similar to that in deep near-IR imaging (Hunt et al. 2003) and broad band optical optical imaging (Izotov & Thuau 2004). The NW component is noticeably more extended and brighter than the SE one. At  $8\mu\text{m}$  the components are still clearly resolved while the contrast in the brightness between the two components has decreased. In normal star forming galaxies the emission sampled by the IRAC  $8\mu\text{m}$  filter is typically dominated by dust continuum, and PAH emission when PAHs are present. Some continuum emission from the nearly Rayleigh-Jeans tail of stellar photospheric emission may also be present, even though its contribution is typically small in late type or irregular galaxies (see Smith et al. 2007). As we discuss

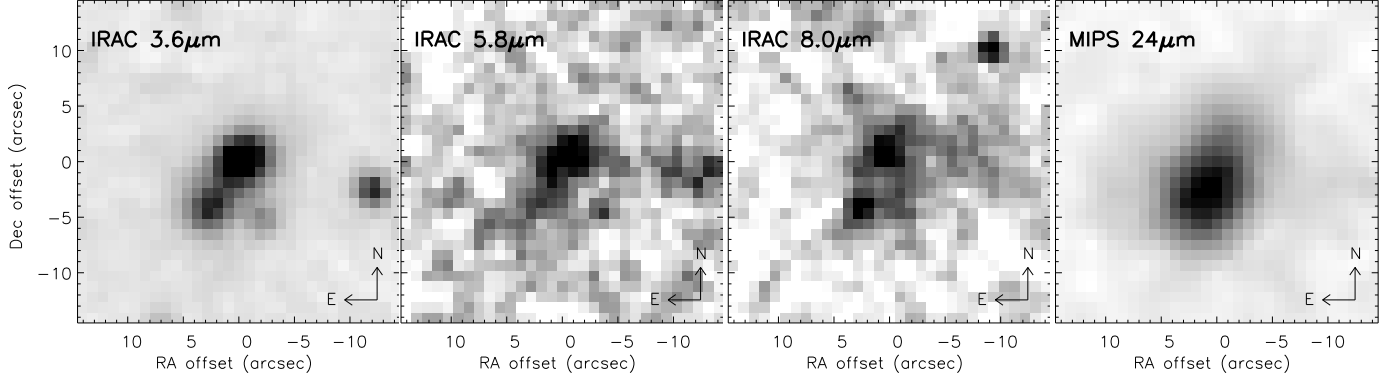


FIG. 1.— IRAC 3.6, 5.8, 8  $\mu\text{m}$  and MIPS 24  $\mu\text{m}$  images of I Zw 18 as observed by *Spitzer*. The galaxy is resolved into a NW and a SE component at 3.6  $\mu\text{m}$  which gradually become blended to a single extended source at 24  $\mu\text{m}$ . At the distance of 12.6 Mpc, 1'' corresponds to  $\sim 61$  pc. The image is centered on the optical centroid of the galaxy ( $\alpha = 09^{\circ}34'02.0''$ ,  $\delta = 55^{\circ}14'28''$ ). Note the change in morphology and peak of the emission as the wavelength increases.

in the following section, no PAH features are detected in the IRS spectrum of I Zw 18 down to our  $1\sigma \sim 0.2$  mJy sensitivity limit. To estimate the contribution of the stellar continuum to the observed 8  $\mu\text{m}$  flux density we follow the approach of Jackson et al. (2006) and apply a scale factor of 0.4 in the 4.5  $\mu\text{m}$  emission from the galaxy. This suggests that no more than  $\sim 25\%$  of the 8  $\mu\text{m}$  flux can be attributed to the stars (Engelbracht et al. 2005). This was also to be expected given the observed steeply rising slope of the mid-IR spectrum. Therefore most of the “mainbody” emission seen in the 8  $\mu\text{m}$  band is due to dust continuum emission. Hence we interpret this gradual shift in brightness from the NW to the SE component to the probable presence of more embedded star formation in the SE component which was obscured in the optical broad band imaging. Interestingly, while optical recombination line ratios give an average extinction of only  $A_V \sim 0.2$  mag, there are also statistically significantly high  $\text{H}\alpha/\text{H}\beta$  flux ratios ( $\sim 3.4$ , corresponding to  $A_V \sim 0.5$  mag) in the SE component (Cannon et al. 2002), suggesting the existence of an appreciable amount of dust within the galaxy. Moreover, as can be seen in Figure 2, there is some extended 8  $\mu\text{m}$  emission, though at low levels, to the west of the NW component. This emission has similar morphology as the radio continuum emission detected in the X-band and L-band by Cannon et al. (2005) and Hunt et al. (2005b), which has been attributed to low-frequency flux from a synchrotron halo.

In Figure 2, we show contour overlays of the 8  $\mu\text{m}$  and 24  $\mu\text{m}$  emission on the *HST* V-band image of the “main body” of I Zw 18. At 8  $\mu\text{m}$ , the source is clearly resolved into two components. The centroids of the two components, especially the NW one, are slightly displaced from their optical counterparts. Moreover, this displacement becomes even more pronounced at longer wavelengths. At 24  $\mu\text{m}$ , the two components are blended into a single source, the centroid of which is located slightly closer to the SE region. This displacement is real and indicates the presence of more 24  $\mu\text{m}$  dust emission in the SE cluster. To confirm this change in morphology we convolved the 8  $\mu\text{m}$  image to the  $\sim 5.4''$  size of the 24  $\mu\text{m}$  point-spread-function (PSF). Even though the resulting marginally resolved source is also elongated in the SE to NW direction, the peak emission was further to the NW than the

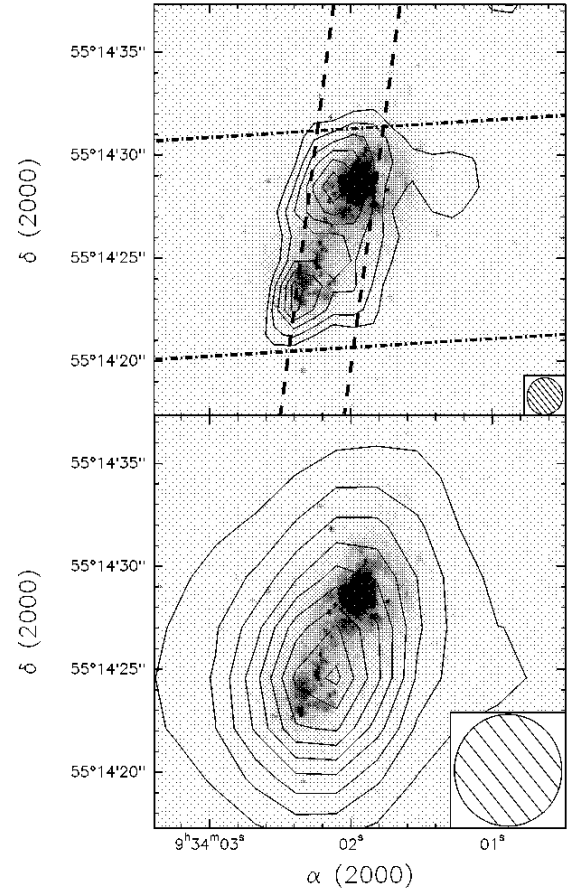


FIG. 2.— a) Top: Contour overlay of the IRAC 8  $\mu\text{m}$  image on the *HST*/WFPC2 F555W image taken from the *HST* archive. The astrometric calibration of the *HST* image has been derived using stars from the U.S. Naval Observatory Astrometric Catalog B1.0, and is the same image as used in Hunt et al. (2005b). The contours range from  $4\sigma$  ( $\sigma = 0.03$  MJy  $\text{sr}^{-1}$ ) above the sky level (1.40 MJy  $\text{sr}^{-1}$ ) to the peak value of 1.71 MJy  $\text{sr}^{-1}$ . The location of the IRS SL (3.6'' in width) and LL (10.5'') slits, are also indicated with the dashed and dash-dotted lines respectively. Note that due to the extent of the galaxy, and the fixed position angle of the slit, part of both the NW and SE components are not fully covered by the SL slit. The size of the PSF at 8  $\mu\text{m}$  (1.8'') is also shown at the lower right of the panel. b) Bottom: the same optical image with the contours of MIPS 24  $\mu\text{m}$  emission (from  $4\sigma$  and above). The size of the PSF is 5.4''.

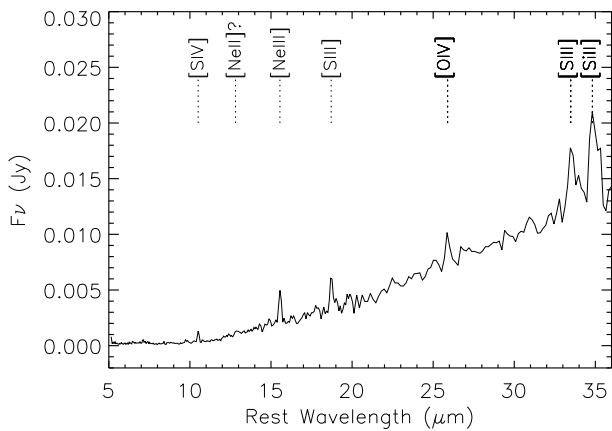


FIG. 3.— *Spitzer/IRS* 5-36  $\mu\text{m}$  low-resolution spectrum of I Zw 18. No scaling factors have been applied to stitch the different orders and modules. We indicate several of the well known mid-IR fine structure emission lines, detected in the spectrum (see also Fig. 4).

peak of the 24  $\mu\text{m}$  image. This suggests an actual change in the spatial distribution of the various dust temperature components in the galaxy. In Figure 2, we also overlay the IRS SL/LL slit on the image of the galaxy. As one can see, since the SL slit is only 3.6'' wide, some of the flux from both components is not properly sampled, resulting in an underestimate of the extended emission from the galaxy. However, because the spectrograph is not sensitive to the low-surface brightness emission from the areas denoted by the lowest 8  $\mu\text{m}$  contours, this does not bias our analysis of the global spectral properties of the system or affects any of the conclusions drawn.

### 3.2. Mid-IR Spectral Features

Figure 3 shows the 5.3-36  $\mu\text{m}$  low-resolution spectrum of I Zw 18 as observed by the IRS. The SNR is  $\sim 3$  times higher than that shown by Wu et al. (2006). As we will discuss in §3.4, the global shape of the mid-IR spectrum, reveals that the IRS spectrum of I Zw 18 continues to rise steeply with wavelength from 5  $\mu\text{m}$  all the way to 36  $\mu\text{m}$ . This is unlike the case of SBS 0335-052E (Houck et al. 2004b), the third lowest metallicity galaxy to date, which has a nearly flat continuum peaking at  $\sim 28 \mu\text{m}$  in  $f_\nu$ .

The improved SNR of the new spectrum enables us to detect for the first time several mid-IR forbidden lines. Fine structure lines, such as [SIV] at 10.51  $\mu\text{m}$  and [NeIII] at 15.55  $\mu\text{m}$  can clearly be seen, even in the low-resolution spectrum. Several additional forbidden lines, such as [NeII] at 12.81  $\mu\text{m}$ , [SIII] at 18.71 and 33.48  $\mu\text{m}$ , as well as [SiII] at 34.82  $\mu\text{m}$  are identified in the high-resolution spectrum (see Figure 4). [OIV] at 25.89  $\mu\text{m}$  and [FeII] at 25.99  $\mu\text{m}$  are blended in LL, but can clearly be resolved in LH. The line fluxes measured from the IRS high-resolution spectrum are reported in Table 2. The observed line ratio of [NeIII]/[NeII] is  $\sim 5$  and the ratio of [SIV]/[SIII](18.71  $\mu\text{m}$ ) is  $\sim 2$ . This indicates that the radiation field in I Zw 18 is much harder than in a typical starburst galaxy, where [NeIII]/[NeII] is usually  $\leq 1$  (Brandl et al. 2006), and even harder than the majority of the BCDs observed so far (Hunt et al. 2006; Wu et al. 2006).

As was the case with SBS 0335-052E, the 5-15  $\mu\text{m}$  spec-

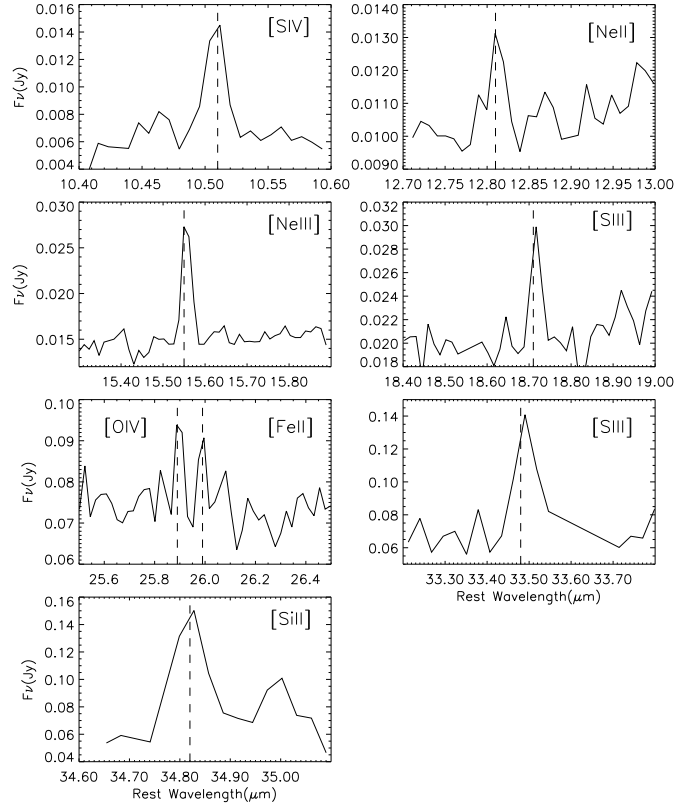


FIG. 4.— Mid-IR fine structure lines of [SIV] (10.51  $\mu\text{m}$ ), [NeII] (12.81  $\mu\text{m}$ ), [NeIII] (15.55  $\mu\text{m}$ ), [SIII] (18.71, 33.42  $\mu\text{m}$ ), [OIV] (25.89  $\mu\text{m}$ ), [FeII] (25.99  $\mu\text{m}$ ) and [SiII] (34.82  $\mu\text{m}$ ) from the high-resolution spectrum of I Zw 18. Note that the sky emission has not been subtracted.

trum of I Zw 18 does not show any detectable Polycyclic Aromatic Hydrocarbon (PAH) emission. Using the new mid-IR spectrum, we measure a  $3\sigma$  upper limit of  $3.5 \times 10^{-22} \text{ W cm}^{-2}$  for the 6.2  $\mu\text{m}$  PAH feature, as well as an equivalent width (EW) of  $< 0.23 \mu\text{m}$ . The 11.2  $\mu\text{m}$  PAH emission has an upper limit of  $1.3 \times 10^{-22} \text{ W cm}^{-2}$  and EW of  $< 0.12 \mu\text{m}$ . The decreasing strength of the PAH features in low metallicity environment is a current topic of interest (see Engelbracht et al. 2005; Wu et al. 2006; O'Halloran et al. 2006; Jackson et al. 2006; Madden et al. 2006; Beirão et al. 2006). The exact reason why PAHs tend to be absent in low-metallicity, high-excitation star-forming regions is not yet clear, although it almost certainly has to do with a combination of several effects, such as low carbon abundance, shock destruction of grains by supernovae, high ionization or excitation resulting from low metallicity and/or extreme radiation field intensity.

### 3.3. Neon and Sulfur Abundances

The fine-structure lines of sulfur and neon measured in the high-resolution spectrum can be used to derive the ionic abundances relative to hydrogen. To derive these abundances one needs at least one hydrogen recombination line (usually H $\beta$ ), as well as an estimate of the electron temperature ( $T_e$ ) and electron density ( $N_e$ ). The H $\beta$  fluxes for I Zw 18 reported in the literature often correspond to small regions of the galaxy or of one of the two components. The IRS SH slit

from which the IR lines were measured contains part of both components. We derive the  $H\beta$  flux from the thermal component of the 3.6 cm continuum (Cannon et al. 2005), which is not affected by extinction effects and encompasses the entire “main body”. The SH slit includes  $\sim 52\%$  of the total  $H\beta$  emission and this gives an  $H\beta$  flux of  $6.1 \times 10^{-14} \text{ ergs cm}^{-2} \text{s}^{-1}$ . The reported electron temperatures in the literature range from 18 000 to 20 000 K for O II and O III (Skillman & Kennicutt 1993; Izotov & Thuan 1999; Thuan & Izotov 2005; Shi et al. 2005), with a slightly lower value for S II ( $T_e \sim 15\,500$  K). The infrared lines are less sensitive to  $T_e$  and here we adopt an average temperature of 19 000 K. An electron density ( $N_e$ ) of  $100 \text{ cm}^{-3}$  was assumed (Shi et al. 2005; Izotov & Thuan 1999). Using the above quantities and resolving the population of the levels for each ion, the ionic abundances can be derived (see Bernard Salas et al. (2001), their eq. 1).

The calculated ionic abundances are presented in Table 2. The elemental abundances can be obtained by adding the contribution of each ion. In the case of neon, only Ne II and Ne III are observed. The presence of O IV suggests that some Ne IV may be present. Assuming that the contribution of Ne IV is 10% of that of Ne III as has been found in some planetary nebulae (PN<sup>8</sup>, Bernard-Salas et al. (2003)), the total neon abundance is  $5.3 \times 10^{-6}$ , which is  $1/23 Z_\odot$ . Similarly, adding up the ionic abundance of S III and S IV, the total sulfur abundance is  $4.0 \times 10^{-7}$ , which is  $1/35 Z_\odot$ . However, this might be a lower limit because sulfur abundance as derived from galactic planetary nebulae and HII regions is lower than the solar sulfur abundance (Pottasch & Bernard-Salas 2006; Maciel & Costa 2003), probably due to an overestimate of the solar value. Comparing directly with the ionic abundance from the optical (Izotov & Thuan 1999), our Ne III abundance is nearly twice as high while S III abundance agrees quite well. The difference in Ne III could come from the electron temperature that is used to derived the ionic abundance. The optical is more affected by the change in temperature as compared to the infrared. Lowering  $T_e$  from 19 000 K to 15 000 K would double the Ne III abundance derived from the 3869 Å line. It is known that in some PN, the temperature obtained from the Ne III ion is lower than that from the O III (Bernard Salas et al. 2002). Another possible explanation is that there are some regions with dust obscuring the optical emission lines. Overall, the neon ( $1/23 Z_\odot$ ) and sulfur ( $1/35 Z_\odot$ ) abundances we derive using the infrared lines are consistent with the nebular oxygen abundance ( $1/30 Z_\odot$ ), which supports the low extinction ( $A_V=0.2$  mag) derived from hydrogen recombination lines by Cannon et al. (2002).

#### 3.4. Comparison with SBS 0335-052E and NGC7714

I Zw 18 and SBS 0335-052E share some properties but are very different in other aspects. Perhaps the most salient difference between their spectral energy distribution (SED) is the fraction of their luminosities emitted in the IR. Using the 15  $\mu\text{m}$  and 30  $\mu\text{m}$  flux densities of I Zw 18 and applying an empirical relation in starburst galaxies (Brandl et al. 2006), we derive

<sup>8</sup> The high excitation and densities in BCDs are a closer match to PN than the typical H II regions found in normal starburst galaxies.

TABLE 2  
FLUXES AND IONIC ABUNDANCES<sup>a</sup>

| $\lambda_{\text{rest}}$ | Feature  | Obs. Flux <sup>b</sup> | $N_{\text{ion}}/N_p$ <sup>c</sup> |
|-------------------------|----------|------------------------|-----------------------------------|
| 10.51                   | [S IV]   | $4.8 \pm 0.3$          | $1.3 \times 10^{-7}$              |
| 12.81                   | [Ne II]  | $0.9 \pm 0.1$          | $1.4 \times 10^{-6}$              |
| 15.55                   | [Ne III] | $4.6 \pm 0.2$          | $3.6 \times 10^{-6}$              |
| 18.71 <sup>d</sup>      | [S III]  | $2.3 \pm 0.2$          | $2.8 \times 10^{-7}$              |
| 25.89                   | [O IV]   | $4.9 \pm 0.3$          | ...                               |
| 25.99                   | [Fe II]  | $3.4 \pm 0.3$          | ...                               |
| 33.48 <sup>d</sup>      | [S III]  | $12.0 \pm 1.2$         | ...                               |
| 34.82                   | [Si II]  | $15.8 \pm 1.8$         | ...                               |

<sup>a</sup> Only the abundances of ions used to calculate the metallicities in this work are listed in this table.

<sup>b</sup> In units of  $10^{-15} \text{ erg cm}^{-2} \text{s}^{-1}$ .

<sup>c</sup> Ionic abundance relative to hydrogen.

<sup>d</sup> Here we use the [S III] at 18.71  $\mu\text{m}$  when calculating the sulfur abundance because this line is in the SH module and provides us a more reliable measurement as compared to the 33.48  $\mu\text{m}$  line which is at the edge of the LH module and is noisy.

$L_{\text{IR}}=1.8 \times 10^7 M_\odot$ . While SBS 0335-052E has  $L_{\text{IR}} \sim 10^9 L_\odot$  and  $L_{\text{IR}}/L_B \sim 1.3$ , I Zw 18 has  $L_{\text{IR}} \sim 10^7 L_\odot$  and  $L_{\text{IR}}/L_B \sim 0.3$ ; the relative infrared luminosity is a factor of 4 times greater in SBS 0335-052E. Another important difference in the infrared SEDs of I Zw 18 and SBS 0335-052E is the peak wavelength of the SED. The SED of SBS 0335-052E peaks at  $\sim 28 \mu\text{m}$  in  $f_\nu$  space (Houck et al. 2004b), indicating very little cold dust. I Zw 18 has a clear detection of  $34 \pm 2.4 \text{ mJy}$  at 70  $\mu\text{m}$  (Engelbracht et al. 2007, in preparation), and the ratio of  $f_{70}/f_{24}$  is more than a factor of 5 while the same ratio in SBS 0335-052 is less than 1. This suggests that contrary to SBS 0335-052E, which is a similarly low metallicity BCD, there is a significant amount of cold dust in I Zw 18.

We can further compare the properties of I Zw 18 with higher-luminosity and more metal-rich starbursts. In Figure 5, we present the spectra of I Zw 18 and SBS 0335-052E, together with a typical starburst galaxy, NGC7714 (Brandl et al. 2004), all of which have been normalized to the flux density of I Zw 18 at 22  $\mu\text{m}$ . Setting aside the strong PAH emission features present in NGC7714, there is a striking similarity between the mid-IR continuum of I Zw 18 and NGC7714, although the latter has a metallicity of more than half solar. At short mid-IR wavelengths ( $\lambda < 10 \mu\text{m}$ ), the warm dust component dominates and it does not change much even for an extended starburst galaxy (Brandl et al. 2006). At longer wavelengths, emission from larger cooler grains is dominant. After normalization at 22  $\mu\text{m}$ , the 70  $\mu\text{m}$  flux of I Zw 18 differs less than 20% when compared to the 70  $\mu\text{m}$  flux of 9.53 Jy (Engelbracht, private communication) or the *IRAS* 60  $\mu\text{m}$  flux of 11.16 Jy for NGC7714. Figure 5 suggests that similarly low metallicity galaxies can have both very flat or very steep spectral slope, while in the latter case, the spectral slope can be as steep as that of a typical starburst. This leads us to conclude that metallicity is not the main parameter driving the difference in the shape of the mid-IR spectral slope (Wu et al. 2006) and the infrared part of the SEDs.

Based on the new Spitzer measurements of the mid- and far-infrared emission from I Zw 18 one could in principle attempt to model the global SED of the galaxy. We did explore this avenue using modelling tools such as

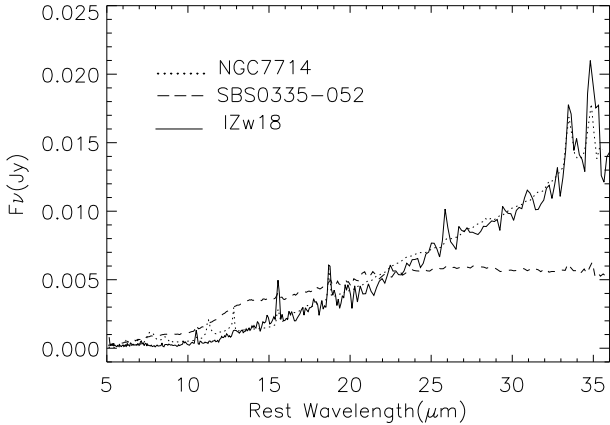


FIG. 5.— The mid-IR spectra of I Zw 18, SBS 0335-052E and NGC7714 between 5-36  $\mu\text{m}$ . The spectra have been normalized to the flux density of I Zw 18 at 22  $\mu\text{m}$ . SBS 0335-052E stands out as having a very flat continuum in the mid-IR, indicating there is much less cold dust in this galaxy. I Zw 18 and NGC7714 display a striking resemblance in this wavelength range.

DUSTY (Ivezić et al. 1999), but with only limited success. The complex geometry of I Zw 18 and the large number of free parameters in the available models prevented us from significantly constraining the physical conditions of the dust. We thus refrain from elaborating on these results until more data are available.

#### 4. STAR FORMATION RATE IN IZW 18

Deriving the star formation rate in nearby galaxies from various observational indicators and understanding the possible variations in the results is extremely useful for “predicting” the properties of high-redshift galaxy populations, where only sparse data are available. Using the available data, we calculated the SFRs of I Zw 18 from different indicators and we present our results in Table 3.

The SFR estimated from the  $\text{H}\alpha$  luminosity gives a value of  $0.05 \text{ M}_\odot \text{ yr}^{-1}$  (Kennicutt et al. 1994; Cannon et al. 2002). However, I Zw 18 has only  $1/30 \text{ Z}_\odot$  and lower metallicities may result in a reduced SFR for a given  $\text{H}\alpha$  luminosity (Lee et al. 2002; Rosenberg et al. 2006). Using the metallicity correction recipe of Lee et al. (2002), the SFR would be  $\sim 0.03 \text{ M}_\odot \text{ yr}^{-1}$ .

The radio continuum emission is another important diagnostic of star-formation process and it is not affected by dust extinction effects. The thermal free-free emission is a direct indicator of SFR and it is typically only  $\sim 10\%$  of the total radio continuum at 1.4 GHz for normal galaxies (Condon 1992). However, in I Zw 18, the fraction of thermal component is three times the typical value ( $\sim 30\%$ : Hunt et al. 2005b; Cannon et al. 2005). Using the relation between radio free-free emission and SFR, we derive a  $\text{SFR} = 0.1 \text{ M}_\odot \text{ yr}^{-1}$  (Hunt et al. 2005b). The non-thermal component of the radio continuum can also be used to calculate SFR and we derive a SFR of  $0.03 \text{ M}_\odot \text{ yr}^{-1}$  (Condon 1992), a factor of 3 lower than the thermally-derived SFR. This difference is a direct consequence of the unusual value of the “thermal/non-thermal” fraction in I Zw 18. This is an important caveat that should be considered when applying the standard

TABLE 3  
STAR FORMATION RATE ESTIMATES OF  
I Zw 18

| SFR indicator                            | SFR<br>( $\text{M}_\odot \text{ yr}^{-1}$ ) | Reference <sup>a</sup> |
|--|---|------------------------|
| $\text{L}_{\text{H}\alpha}$ <sup>b</sup> | 0.05  | (1)                    |
| $\text{L}_{\text{H}\alpha}$ <sup>c</sup> | 0.03  | (2)                    |
| $\text{L}_{\text{TIR}}$                  | 0.003                                       | (3)                    |
| $\text{L}_{24\mu\text{m}}$               | 0.006                                       | (4)                    |
| $\text{L}_{\text{IR}+\text{UV}}$         | 0.02  | (5)                    |
| $\text{L}_{\text{thermal}}$              | 0.1   | (6)                    |
| $\text{L}_{\text{non-thermal}}$          | 0.03  | (6)                    |

<sup>a</sup> References: 1) Kennicutt et al. (1994), 2) Lee et al. (2002) 3) Kennicutt (1998) 4) Wu et al. (2005) 5) Bell et al. (2005) 6) Condon (1992).

<sup>b</sup> Not corrected for low-metallicity effects.

<sup>c</sup> After correcting the low-metallicity effects.

correlations, which have been established for normal star forming galaxies, in very young low-metallicity systems.

Finally, the SFRs estimated from the infrared are significantly lower. Using the total infrared luminosity of  $1.8 \times 10^7 \text{ L}_\odot$ , we derive a  $\text{SFR} = 0.003 \text{ M}_\odot \text{ yr}^{-1}$  (Kennicutt 1998), while using the  $24 \mu\text{m}$  emission, we find that  $\text{SFR} = 0.006 \text{ M}_\odot \text{ yr}^{-1}$  (Calzetti et al. 2005; Wu et al. 2005). This is probably because the dust content in I Zw 18 is so low while the above relations have been calibrated for sources of high optical depth, where virtually all of the UV radiation is converted to infrared luminosity. A simple calculation using the reddening curve of the Small Magellanic Cloud assuming an  $\text{A}_\text{V} = 0.2$  mag suggests that a significant amount of UV light has leaked out without being absorbed by the dust, thus the lower SFRs estimated from the infrared are not unexpected. The readers should be aware of these complications when applying the canonical infrared relations for estimating the SFR in environments with low dust optical depth. If we were to assume that  $\text{L}_{\text{IR}}$  accounts for the bolometric luminosity of the obscured populations while  $\text{L}_{\text{UV}}$  (Kinney et al. 1993) represents the contribution of the unobscured stars, and use the eq.1 of Bell et al. (2005)<sup>9</sup>, we find a SFR of  $0.02 \text{ M}_\odot \text{ yr}^{-1}$ , more consistent with the SFRs derived using the  $\text{H}\alpha$  or radio luminosities.

#### 5. CONCLUSIONS

We have explored the mid-IR and far-IR properties of the archetype BCD I Zw 18 based on Spitzer data:

1. Using the low-resolution modules of the IRS, we have acquired the deepest mid-IR spectrum of this galaxy obtained so far. No PAH emission is found which confirms the absence of PAHs in low metallicity systems. However, the mid- to far-IR spectral slope of I Zw 18 is surprisingly similar to NGC 7714, a typical starburst galaxy with half solar metallicity. This, especially the MIPS  $70 \mu\text{m}$  detection, would suggest the presence of a significant amount of cold dust in I Zw 18.

2. Variations in the morphology of the galaxy from 3.6 to  $24 \mu\text{m}$  imaging imply that more dust emission is present in its SE component than in the NW one. This agrees well with the results of Cannon et al. (2002).

<sup>9</sup>  $\text{SFR} = 9.8 \times 10^{-11} (\text{L}_{\text{IR}} + 2.2 \text{ L}_{\text{UV}})$

3. The mid-IR fine-structure lines identified in the high-resolution spectrum of I Zw 18 imply a neon and sulfur abundance of 1/23 and 1/35  $Z_{\odot}$  respectively, consistent with the optically derived oxygen abundance of 1/30  $Z_{\odot}$ .

4. Estimates of the star formation rates calculated from different indicators show considerable scatter.  $L_{\text{IR}}$  and  $L_{24\mu\text{m}}$  give lower SFRs when compared with results using  $\text{H}\alpha$  or  $L_{1.4\text{GHz}}$ , probably because the low dust content in this galaxy can only convert a small fraction of the UV radiation emitted by stars into  $L_{\text{IR}}$ . This should be considered when interpreting star formation rates de-

rived for high-redshift low metallicity galaxies.

We thank Chad Engelbracht for graciously providing the IRAC and MIPS photometric measurements for our source before publishing the data. We also thank Rob Kennicutt for insightful discussions. We thank the anonymous referee, whose careful reading and detailed comments greatly improved this manuscript. Support for this work was provided by NASA through Contract Number 1257184 issued by JPL/Caltech.

#### REFERENCES

Allende Prieto, C., Lambert, D. L., & Asplund, M. 2001, *ApJ*, 556, L63

Aloisi, A. et al. 2007, *astro-ph/0702216*

Aloisi, A., Tosi, M., & Greggio, L. 1999, *AJ*, 118, 302

Anders, E. & Grevesse, N. 1989, *Geochim. Cosmochim. Acta*, 53, 197

Beirão, P., Brandl, B. R., Devost, D., Smith, J. D., Hao, L., & Houck, J. R. 2006, *ApJ*, 643, L1

Bell, E. F., et al. 2005, *ApJ*, 625, 23

Bernard Salas, J., Pottasch, S. R., Feibelman, W. A., & Wesselius, P. R. 2002, *A&A*, 387, 301

Bernard Salas, J., Pottasch, S. R., Beintema, D. A., & Wesselius, P. R. 2001, *A&A*, 367, 949

Bernard-Salas, J., Pottasch, S. R., Wesselius, P. R., & Feibelman, W. A. 2003, *A&A*, 406, 165

Brandl, B. R., et al. 2004, *ApJS*, 154, 188

Brandl, B. R., et al. 2006, *ApJ*, 653, 1129

Calzetti, D., et al. 2005, *ApJ*, 633, 871

Cannon, J. M., Skillman, E. D., Garnett, D. R., & Dufour, R. J. 2002, *ApJ*, 565, 931

Cannon, J. M., Walter, F., Skillman, E. D., & van Zee, L. 2005, *ApJ*, 621, L21

Cohen, M., Megeath, T.G., Hammersley, P.L., Martin-Luis, F., & Stauffer, J. 2003, *AJ*, 125, 2645

Condon, J. J. 1992, *ARA&A*, 30, 575

Dekel, A., & Silk, J. 1986, *ApJ*, 303, 39

Devereux, N. A., & Eales, S. A. 1989, *ApJ*, 340, 708

Engelbracht, C. W., Gordon, K. D., Rieke, G. H., Werner, M. W., Dale, D. A., & Latter, W. B. 2005, *ApJ*, 628, L29

Fazio, G. G., et al. 2004, *ApJS*, 154, 10

Higdon, S. J. U., et al. 2004, *PASP*, 116, 975

Hirashita, H., & Hunt, L. K. 2004, *A&A*, 421, 555

Hopkins, A. M., Schulte-Ladbeck, R. E., & Drozdovsky, I. O. 2002, *AJ*, 124, 862

Houck, J. R., et al., 2004, *ApJS*, 154, 18

Houck, J. R., et al., 2004, *ApJS*, 154, 211

Hunt, L. K., Thuan, T. X., & Izotov, Y. I. 2003, *ApJ*, 588, 281

Hunt, L., Bianchi, S., & Maiolino, R. 2005a, *A&A*, 434, 849

Hunt, L. K., Dyer, K. K., & Thuan, T. X. 2005b, *A&A*, 436, 837

Hunt, L. K., Thuan, T. X., Sauvage, M., Izotov, Y. I., 2006, *ApJ*, in press, *astro-ph/0610405*

Hunter, D. A., & Thronson, H. A., Jr. 1995, *ApJ*, 452, 238

Ivezic, Z., Nenkova, M., & Elitzur, M. 1999, User Manual for *DUSTY*, University of Kentucky Internal Report, accessible at <http://www.pa.uky.edu/~moshe/dusty>

Izotov, Y. I., Foltz, C. B., Green, R. F., Guseva, N. G., & Thuan, T. X. 1997, *ApJ*, 487, L37

Izotov, Y. I. & Thuan, T. X. 1999, *ApJ*, 511, 639

Izotov, Y. I., Chaffee, F. H., Foltz, C. B., Thuan, T. X., Green, R. F., Papaderos, P., Fricke, K. J., & Guseva, N. G. 2001, *ApJ*, 560, 222

Izotov, Y. I., & Thuan, T. X. 2004, *ApJ*, 616, 768

Izotov, Y. I., Thuan, T. X., & Guseva, N. G. 2005, *ApJ*, 632, 210

Jackson, D. C., Cannon, J. M., Skillman, E. D., Lee, H., Gehrz, R. D., Woodward, C. E., & Polomski, E. 2006, *ApJ*, 646, 192

Kennicutt, R. C., Jr. 1998, *ARA&A*, 36, 189

Kennicutt, R. C., Jr., Tamblyn, P., & Congdon, C. E. 1994, *ApJ*, 435, 22

Kinney, A. L., Bohlin, R. C., Calzetti, D., Panagia, N., & Wyse, R. F. G. 1993, *ApJS*, 86, 5

Klein, U., Weiland, H., & Brinks, E. 1991, *A&A*, 246, 323

Kunth, D. & Östlin, G. 2000, *A&A Rev.*, 10, 1

Lee, J. C., Salzer, J. J., Impey, C., Thuan, T. X., & Gronwall, C. 2002, *AJ*, 124, 3088

Maciel, W. J., & Costa, R. D. D. 2003, *IAU Symposium*, 209, 551

Madden, S. C., Galliano, F., Jones, A. P., & Sauvage, M. 2006, *A&A*, 446, 877

Maiolino, R., Juarez, Y., Mujica, R., Nagar, N. M., & Oliva, E. 2003, *ApJ*, 596, L155

Monamy, Y., et al. 2005, *A&A*, 439, 111

Östlin, G. 2000, *ApJ*, 535, L99

O'Halloran, B., Satyapal, S., & Dudik, R. P. 2006, *ApJ*, 641, 795

Papaderos, P., Izotov, Y. I., Guseva, N. G., Thuan, T. X., & Fricke, K. J. 2006, *A&A*, 454, 119

Pottasch, S. R., & Bernard-Salas, J. 2006, *A&A*, 457, 189

Recchi, S., Matteucci, F., D'Ercole, A., & Tosi, M. 2002, *A&A*, 384, 799

Rieke, G. H., et al. 2004, *ApJS*, 154, 25

Rosenberg, J. L., Ashby, M. L. N., Salzer, J. J., & Huang, J.-S. 2006, *ApJ*, 636, 742

Searle, L., & Sargent, W. L. W. 1972, *ApJ*, 173, 25

Shi, F., Kong, X., Li, C., & Cheng, F. Z. 2005, *A&A*, 437, 849

Skillman, E. D., & Kennicutt, R. C., Jr. 1993, *ApJ*, 411, 655

Smith, J.D. T., et al. 2007, *ApJ* (in press *astro-ph/0610913*)

Thuan, T. X., & Izotov, Y. I. 2005, *ApJS*, 161, 240

van Zee, L., Westpfahl, D., Haynes, M. P., & Salzer, J. J. 1998, *AJ*, 115, 1000

Weedman, D. W., Le Floc'h, E., Higdon, S. J. U., Higdon, J. L., & Houck, J. R. 2006, *ApJ*, 638, 613

Werner, M., et al. 2004, *ApJS*, 154, 1

White, S. D. M., & Rees, M. J. 1978, *MNRAS*, 183, 341

Wu, H., Cao, C., Hao, C.-N., Liu, F.-S., Wang, J.-L., Xia, X.-Y., Deng, Z.-G., & Young, C. K.-S. 2005, *ApJ*, 632, L79

Wu, Y., Charmandaris, V., Hao, L., Brandl, B. R., Bernard-Salas, J., Spoon, H. W. W., & Houck, J. R. 2006, *ApJ*, 639, 157

Zwicky, F. 1966, *ApJ*, 143, 192